Journal of Magnetic Resonance 207 (2010) 304–311

Contents lists available at ScienceDirect

Journal of Magnetic Resonance

journal homepage: www.elsevier.com/locate/jmr

Qualitative and quantitative ultrashort echo time (UTE) imaging of cortical bone

Jiang Du [a,*], Michael Carl [b], Mark Bydder [a], Atsushi Takahashi [b], Christine B. Chung [a], Graeme M. Bydder [a]

[a] Department of Radiology, University of California, San Diego, United States
[b] Global Applied Science Laboratory, GE Healthcare, 333 Ravenswood Ave. Bldg. 307, Menlo Park, CA 94025, United States

ARTICLE INFO

Article history:
Received 20 March 2010
Revised 15 September 2010
Available online 25 September 2010

Keywords:
Ultrashort TE
Projection reconstruction
Adiabatic inversion
Bone water concentration
Relaxation times

ABSTRACT

We describe the use of two-dimensional ultrashort echo time (2D UTE) sequences with minimum TEs of 8 μs to image and quantify cortical bone on a clinical 3T scanner. An adiabatic inversion pulse was used for long T_2 water and fat signal suppression. Adiabatic inversion prepared UTE acquisitions with varying TEs were used for T_2^* measurement. Saturation recovery UTE acquisitions were used for T_1 measurement. Bone water concentration was measured with the aid of an external reference phantom. UTE techniques were evaluated on cadaveric specimens and healthy volunteers. A signal-to-noise ratio of around 30, contrast-to-noise ratio of around 27/20 between bone and muscle/fat were achieved in tibia in vivo with a nominal voxel size of $0.23 \times 0.23 \times 6.0$ mm^3 in a scan time of 5 min. A mean T_1 of 223 ± 11 ms and mean T_2^* of 390 ± 19 μs were found. Mean bone water concentrations of 23.3 ± 1.6% with UTE and 21.7 ± 1.3% with adiabatic inversion prepared UTE sequences were found in tibia in five normal volunteers. The results show that in vivo qualitative and quantitative evaluation of cortical bone is feasible with 2D UTE sequences.

1. Introduction

Conventional magnetic resonance imaging (MRI) pulse sequences with echo times (TEs) of 1 ms or greater provide little or no detectable signal from cortical bone which has an extremely short T_2^* of around 300–500 μs [1,2]. By using half-sinc radiofrequency (RF) pulses, or short hard pulses, radial or spiral mapping of k-space and other techniques, nominal TEs of less than 200 μs can be achieved [1–7]. These two-dimensional (2D) and 3D ultrashort TE (UTE) sequences make it possible to detect signal from cortical bone and directly image and quantify T_1, T_2^* and water concentration of this tissue.

Although bone signal is detectable with UTE sequences, positive visualization of bone for qualitative purposes is limited by the presence of high signals from long T_2 water and fat. To reduce the signals from these tissues a typical approach is to use one or two saturation pulses (usually SINC or Gaussian pulses) followed by dephasing gradients [8–10]. However, both SINC and Gaussian pulses are sensitive to B1 inhomogeneity. As a consequence the residual long T_2 water and especially fat signals may be similar to or even higher than those from cortical bone [11,12], thereby compromising bone contrast. An alternative is to use adiabatic pulses which are relatively insensitive to B1 inhomogeneity [13], and have been employed for long T_2 signal suppression using two UTE acquisitions: one with, and the other without adiabatic inversion recovery (IR) preparation [14]. Addition of the two UTE data sets can then be used to selectively suppress long T_2 signals. However, a scaling factor is needed to compensate for T_1 effects and ensure that the inverted long T_2 magnetization approximates the noninverted magnetization in order to achieve complete long T_2 signal cancellation. This procedure is complicated further if there are multiple long T_2 species with different T_1 components.

There are also significant problems in quantitative evaluation of cortical bone using UTE sequences. 3D UTE sequences are time consuming and thus problematic for T_1 and T_2^* quantification in vivo. 2D UTE sequences are subject to eddy currents leading to a broadened slice profile [3]. The excitation of out-of-slice long T_2 water and fat may significantly distort the exponential T_2^* decay curve, resulting in inaccurate T_2^* estimation [3,15]. T_1 measurement using the saturation recovery technique has been reported [1,2,12], however, the long quantification times may limit its clinical use [12]. UTE provides a non-invasive way of evaluating bone water concentration through comparison of the MR signal from bone with that of an external phantom [2,12], however, this estimation requires reliable, fast and patient-specific T_1 and T_2^* measurements. Errors in these estimations propagate to bone water quantification.

In this paper the problems of qualitative visualization and quantification of cortical bone in the clinical context are addressed using different approaches including basic UTE sequences with TEs as low as 8 μs, adiabatic IR prepared UTE sequences (IR-UTE), and saturation recovery UTE sequences.

* Corresponding author. Address: Department of Radiology, University of California, San Diego, 200 West Arbor Drive, San Diego, CA 92103-8226, United States. Fax: +1 619 471 0503.
E-mail address: jiangdu@ucsd.edu (J. Du).

1090-7807/$ - see front matter © 2010 Elsevier Inc. All rights reserved.
doi:10.1016/j.jmr.2010.09.013

2. Materials and methods

2.1. Pulse sequence

A 2D UTE sequence (Fig. 1a) was implemented on a 3T Signa TwinSpeed scanner (GE Healthcare Technologies, Milwaukee, WI) with gradient capabilities of 150 T/m/s slew rate and 40 mT/m amplitude on each axis. The sequence employed a half-sinc RF pulse (duration = 472 μs, bandwidth = 2.7 kHz), which together with variable rate selective excitation (VERSE) [17], radial ramp sampling and fast transmit/receive switching reduced the nominal TE to 8 μs [18–20]. Bipolar slice selective gradients and readout gradients were employed to help control eddy currents. Eddy currents from the paired positive and negative gradients add destructively, reducing the effective eddy currents. The half RF pulse was applied during the second half of the bipolar slice selection gradient. No signal excitation occurs during the first half of the bipolar gradient, which only helps with eddy currents control. Bipolar readout gradients were used to reduce long term eddy currents effects which may influence the signal of the next TR. The basic 2D UTE sequence was then modified by adding an adiabatic inversion pulse for long T_2 signal suppression, variable TE delays for T_2^* measurement, and a hard 90° pulse for T_1 measurement. Bone water was quantified with the aid of an external reference phantom. The technical details for each approach are discussed below.

2.2. Long T_2 signal suppression

Cortical bone contains about 15–20% free water by volume [16], and has a mobile proton density far below those of muscle (~70%) and fat (~90%). This usually results in higher signals from these tissues. In qualitative studies it is of considerable value to suppress the high signals from long T_2 water and fat in order to increase the conspicuity of bone. To do this an adiabatic fast passage (Silver–Hoult) inversion pulse (duration = 8.6 ms, bandwidth = 1.4 kHz) centered at −220 Hz was used to invert the long T_2 water and fat magnetization. The 2D UTE acquisition was then begun at a delay time (TI) designed to allow the inverted long T_2 water and fat magnetization to closely approach the null point, as shown in Fig. 1b. This type of simultaneous reduction in long T_2 water (such as muscle) and fat signals is complicated by the significant difference in T_1 between muscle (~1400 ms) and fat (~360 ms) at 3T [21]. Because of this the inverted longitudinal magnetization of muscle and fat do not reach the null point simultaneously. To study this problem further simulation of the recovery of long T_2 muscle and fat magnetization after a single adiabatic IR pulse was performed using the following equation:

$$M_{IR} \sim M_0 \times (1-2 \times e^{-TI/T_1} + e^{-TR/T_1}) \quad (1)$$

2.3. T_2^* measurement

The T_2^* of cortical bone has been measured with UTE acquisitions at progressively increasing TEs [1,2,12]. However, the increase in TE results in different effects from time varying eddy currents, including alterations to the slice profile and different degrees of long T_2 signal contamination [3]. As a result, significant errors in T_2^* quantification may be introduced [15]. Efficient long T_2 signal suppression with adiabatic inversion and nulling may significantly reduce out-of-slice long T_2 signal contamination of this type [18]. To assess this problem UTE and IR-UTE acquisitions with progressively increasing TEs were compared for measuring the T_2^* of the mid-diaphyseal tibia of a cadaveric lower leg specimen using the protocols shown in Table 1. Protocol I used basic UTE acquisitions (total scan time of 21 min), and protocol II used IR-UTE acquisitions with fewer projections (total scan time of 10 min). The single exponential signal decay model shown below was used to fit T_2^*:

$$S(TE) = S_0 \times e^{-TE/T_2^*} + C \quad (2)$$

where C accounts for background noise, including pseudo-noise associated with undersampled UTE data acquisitions.

2.4. T_1 measurement

Quantification of T_1 of cortical bone requires the use of UTE sequences because of the tissue's short T_2. Here a non-selective 90° square pulse with a duration of 256 μs (which is limited by the RF system) was followed by a large crusher gradient to saturate signals from both long and short T_2 species. UTE acquisitions with progressively increasing saturation recovery times (TSRs) were then used to detect the recovery of cortical bone longitudinal magnetization. Typically a long TR is used for saturation recovery UTE T_1 quantification as shown in protocol I [12]. However, this approach is very time consuming and impractical for clinical applications. To reduce the total quantification time, a short TR together with a highly undersampled UTE acquisition was used as shown in protocol II. The two protocols were compared for T_1 measurement of mid-diaphyseal tibia in a cadaveric lower leg specimen. The simple exponential signal recovery model shown below was used to fit T_1 [8]:

$$S(TSR) = S_0 \times [1 - (1-k) \times e^{-TSR/T_1}] + C \quad (3)$$

where k accounts for the residual fraction of the longitudinal magnetization of cortical bone after a nominal 90° pulse.

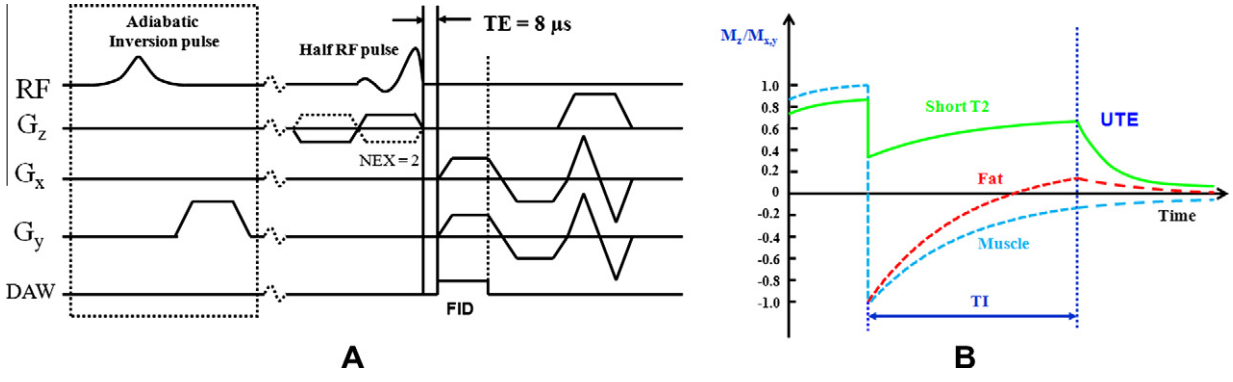

Fig. 1. The 2D UTE sequence. This employs half RF pulse excitations and radial ramp sampling to reduce the nominal TE to 8 μs (A). Long T_2 suppression is achieved with an adiabatic inversion pulse and approximate signal nulling. 2D UTE data acquisition starts when the inverted long T_2 water and fat magnetization approaches the null point. This creates high contrast for cortical bone (B).

Table 1
Protocols for measuring T_1 and T_2^* of cortical bone.

Protocol I					Protocol II				
T_1 measurement			T_2^* measurement		T_1 measurement			T_2^* measurement	
TSR (ms)	TR (ms)	Readout × projection	TE (μs)	Readout × projection	TSR (ms)	TR (ms)	Readout × projection	TE (μs)	Readout × projection
10	1500	512 × 511	8	512 × 511	10	18	512 × 255	8	512 × 255
50	1500	512 × 511	200	512 × 511	50	58	512 × 255	200	512 × 255
100	1500	512 × 511	800	512 × 511	100	108	512 × 255	800	512 × 255
200	1500	512 × 511	1500	512 × 511	200	208	512 × 255	1500	512 × 255
400	1500	512 × 511	TR = 300 ms		400	408	512 × 255	TR = 300 ms	
800	1500	512 × 511			800	808	512 × 255	TI = 120 ms	
Scan time: 154 min			Scan time: 21 min		San time: 14 min			Scan time: 10 min	

2.5. Bone water measurement

Accurate estimation of bone water requires consideration of relaxation, coil sensitivity and slice profile effects. When the duration of half RF pulses is of the order of T_2^*, the transverse magnetization for a steady-state UTE acquisition can be written as [2,8]:

$$\mu_{xy} \propto f_{xy}(b_1(t), T_1, T_2^*) \times \frac{(1 - e^{-\mathrm{TR}/T_1})}{(1 - f_z(b_1(t), T_1, T_2^*) \times e^{-\mathrm{TR}/T_1})} \times e^{-\mathrm{TE}/T_2^*} \quad (4)$$

where f_{xy} and f_z describe the behavior of the transverse magnetization and longitudinal magnetization, respectively, as a function of half pulse $b_1(t)$ as well as the transverse (T_2^*) and longitudinal (T_1) relaxation times of cortical bone.

The bone water concentration (BWC) can be calculated as follows:

$$\mathrm{BWC} = \frac{I_{bone}}{I_{ref}} \times \frac{f_{xy}^{ref}}{f_{xy}^{bone}} \times \frac{(1 - e^{-\mathrm{TR}/T_{1,ref}})}{(1 - e^{-\mathrm{TR}/T_{1,bone}})} \times \frac{(1 - f_z^{bone} \times e^{-\mathrm{TR}/T_{1,bone}})}{(1 - f_z^{ref} \times e^{-\mathrm{TR}/T_{1,ref}})} \times \frac{e^{-\mathrm{TE}/T_{2,ref}}}{e^{-\mathrm{TE}/T_{2,bone}}} \times \frac{\eta_{ref}}{\eta_{bone}} \times \frac{\Gamma_{ref}}{\Gamma_{bone}} \times RWC \quad (5)$$

where RWC is the water concentration of reference phantom, I_{bone} and I_{ref} are the corresponding image intensities, η_{bone} and η_{ref} are the corresponding coil sensitivities, and Γ_{bone} and Γ_{ref} are correction factors for out-of-slice excitation.

The external reference was a mixture of distilled water (20%) and D_2O (80%) doped with 22 mM $MnCl_2$ [12]. The high concentration of $MnCl_2$ reduced T_2^* to around 400 μs and T_1 to around 5 ms. A quadrature knee birdcage coil was used for bone water quantification due to its superior uniformity compared with most surface or phased-array coils. The reference tube was placed close to the midshaft of the tibia, with both close to the coil iso-center. As a result η_{bone} approximates η_{ref}. If we ignore the difference in out-of-slice signal contamination for cortical bone and the reference phantom (i.e., Γ_{bone} approximates Γ_{ref}), and note that TR is much longer than $T_{1,ref}$ and that TE is much shorter than $T_{2,ref}^*$ and $T_{2,bone}^*$, Eq. (6) for bone water concentration can be simplified as follows:

$$\mathrm{BWC_{UTE}} \approx \frac{I_{bone}}{I_{ref}} \times \frac{f_{xy}^{ref}}{f_{xy}^{bone}} \times \frac{(1-e^{-\mathrm{TR}/T_{1,ref}})}{(1-e^{-\mathrm{TR}/T_{1,bone}})} \times \frac{(1-f_z^{bone}\times e^{-\mathrm{TR}/T_{1,bone}})}{(1-f_z^{ref}\times e^{-\mathrm{TR}/T_{1,ref}})} \times \frac{e^{-\mathrm{TE}/T_{2,ref}^*}}{e^{-\mathrm{TE}/T_{2,bone}^*}} \times \mathrm{RWC} \approx \frac{I_{bone}}{I_{ref}} \times \frac{(1-f_z^{bone}\times e^{-\mathrm{TR}/T_{1,bone}})}{(1-e^{-\mathrm{TR}/T_{1,bone}})} \times RWC \quad (6)$$

However, out-of-slice signals from muscle and fat may be included and artifactually increase the measured bone water concentration. In this study we employed an adiabatic IR pulse to suppress signals from muscle and fat. As a result, Γ_{bone} approximated Γ_{ref}. Assuming that the bone signal is attenuated by a factor of P, and introducing $Q = 1 - P$, we can calculate bone water using the following equation (details in Appendix A):

$$\mathrm{BWC_{IR-UTE}} \approx \frac{I_{bone}}{I_{ref}} \times \frac{1 - Q_{bone} \times f_z \times e^{-\mathrm{TR}/T_{1,bone}}}{1 + (Q_{bone} - 1) \times e^{-\mathrm{TI}/T_{1,bone}} - Q_{bone} \times e^{-\mathrm{TR}/T_{1,bone}}} \times \mathrm{RWC} \quad (7)$$

Q is a function of T_1 and T_2^*. It can be derived from Bloch equation simulation once the T_1 and T_2^* of cortical bone have been measured [14].

3. Imaging experiments

3.1. Cadaveric specimen study

The IR-UTE sequence was first applied to the mid-diaphyseal tibia of a human lower leg specimen (with soft tissue intact) for bone contrast optimization. The following imaging parameters were used: FOV = 10 cm, slice thickness = 6 mm, bandwidth = 125 kHz, flip angle = 60°, TR = 300 ms, TE = 8/4400 μs (the second echo was acquired to show the effect of long T_2 signal suppression), reconstruction matrix size = 512 × 512, number of half projections = 899, single slice, four dummy scans to establish equilibrium, total scan time = 9 min. Five different TIs (80, 100, 120, 140 and 160 ms) were used. The optimal TR/TI combination was then used to image the mid-diaphyseal radius and ulna of a cadaveric forearm specimen. Clinical 2D gradient echo (GE) and fast spin echo (FSE) sequences with similar spatial resolution were used for comparison. T_1 and T_2^* quantification were performed on the tibial specimen using the two protocols shown in Table 1. A 3-in. surface coil (receive only) was used for imaging the tibial cortical specimen (the body coil was used for signal excitation). A birdcage transmit/receive coil was used for imaging the radial and ulna cortical specimen.

3.2. In vivo volunteer study

The 2D UTE sequences were also used to image and quantify T_2^*, T_1 and water concentration of the mid-diaphyseal tibia in five healthy volunteers (all males, ranging in age from 24 to 35 years, average age of 29). Written informed consent approved by our Institutional Review Board was obtained prior to their participation in this study. Imaging parameters were similar to those used in the cadaveric study, except for a larger FOV of 12 cm, fewer projections (number of projections = 511) and shorter scan time (5 min as compared to 9 min). The fast protocol II shown in Table 1 was used for T_2^* and T_1 measurements. The 3-in. coil was used for bone morphological imaging as well as T_2^* and T_1 quantification. The quadrature knee transmit/receive coil was used for bone water quantification, with the FOV increased to 21 cm, readout reduced to 256 samples and sampling frequency bandwidth increased to ±125 kHz. Clinical 2D GE and FSE sequences with similar spatial resolution were performed for comparison.

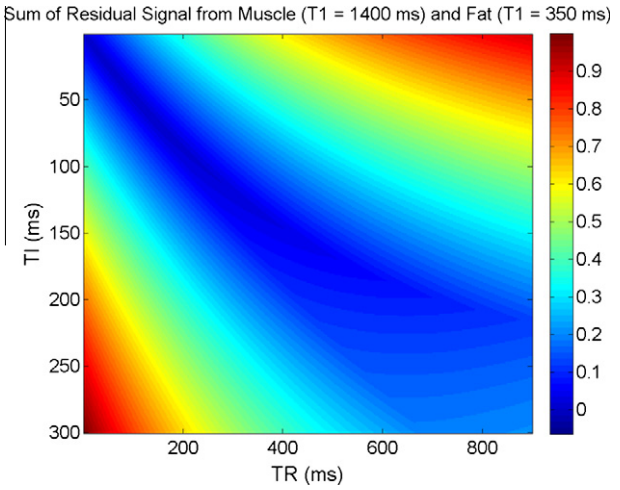

Fig. 2. Simulation of the sum of residual signals from muscle (T_1 = 1400 ms) and fat (T_1 = 350 ms) as a function of inversion time (TI) and repetition time (TR). Appropriate combinations of TR and TI provide greater than 85% long T_2 muscle and fat signal suppression.

3.3. Data analysis

Signal-to-noise ratios (SNRs) and contrast-to-noise ratios (CNRs) were used to evaluate the efficiency of the UTE sequences. SNRs were calculated as the ratio of the mean signal intensity inside a user-drawn region of interest (ROI) to the standard deviation of the background noise. CNRs between cortical bone and muscle and fat were calculated as their signal difference over the background noise. T_2^* and T_1 values were obtained using a Levenberg–Marquardt fitting algorithm based on Eqs. (2) and (3). Bone water concentration was quantified based on Eq. (7) for UTE and Eq. (8) for IR-UTE acquisitions. Five different ROIs placed within the tibial cortex were used to determine the standard deviation of measurements.

4. Results

4.1. Simulation

The efficiency of simultaneous suppression of fat and muscle depends on the choice of TR and TI in IR-UTE imaging, as demonstrated in Fig. 2. The sum of the residual signals from muscle and fat can be reduced by more than 85% through appropriate combinations of TR and TI. The short T_2 magnetization is also affected by the adiabatic IR pulse. Bloch equation simulation showed that the adiabatic IR pulse resulted in about 55% signal reduction for cortical bone ($T_1 \sim 220$ ms, $T_2^* \sim 400$ μs) with a TR of 300 ms and TI of 120 ms, showing that the adiabatic IR-UTE approach is a low signal but high contrast technique. Bloch equation simulation also showed a value of around 0.67 for f_z and 0.11 for Q which were used for subsequent calculations of bone water concentration.

4.2. Cadaveric specimen study

Axial 2D IR-UTE images of the mid-diaphyseal tibia are shown in Fig. 3, which demonstrates that the effectiveness of long T_2 suppression depends on the choice of TR and TI. Table 2 shows measured SNRs as well as CNRs between bone and fat (CNR_{B_F}) and CNRs between bone and muscle (CNR_{B_M}) for different TR and TI combinations. SNR values ranging from 24 to 35 and CNR_{B_M} ranging from 17 to 29 were achieved with TIs ranging from 80 to 160 ms. CNR_{B_F} was high for TIs in the range of 100 to 140 ms with a peak at 120 ms. A TR of 300 ms and TI of 120 ms were used for subsequent studies.

Transverse images of the radius and ulna from a cadaveric forearm are displayed in Fig. 4. The clinical 2D FSE image (Fig. 4A) provides near zero signal from the radius, ulna and tendons. In contrast, the 2D IR-UTE image (Fig. 4B) provided a high SNR of 44 ± 4 for cortical bone, a high CNR of 36 ± 2 between bone and muscle, and a high CNR of 28 ± 2 between bone and marrow fat with a nominal spatial resolution of 0.2 × 0.2 × 6 mm^3 and a total scan time of 9 min.

Fig. 5 shows quantitative evaluation of T_2^* and T_1 for the mid-diaphyseal tibia of a cadaveric lower leg specimen. There was significant distortion in the exponential T_2^* curve using regular UTE acquisitions, where a T_2^* of 1116 ± 643 μs was found with high standard error and low fitting confidence (R^2 = 0.919). In contrast, the IR-UTE approach provided excellent exponential curve fitting, with a T_2^* of 422 ± 13 μs (R^2 = 0.999). There was a small difference in T_1 quantification of less than 5% between saturation recovery UTE acquisitions with a long TR and those with a short TR. The total scan time was reduced by more than

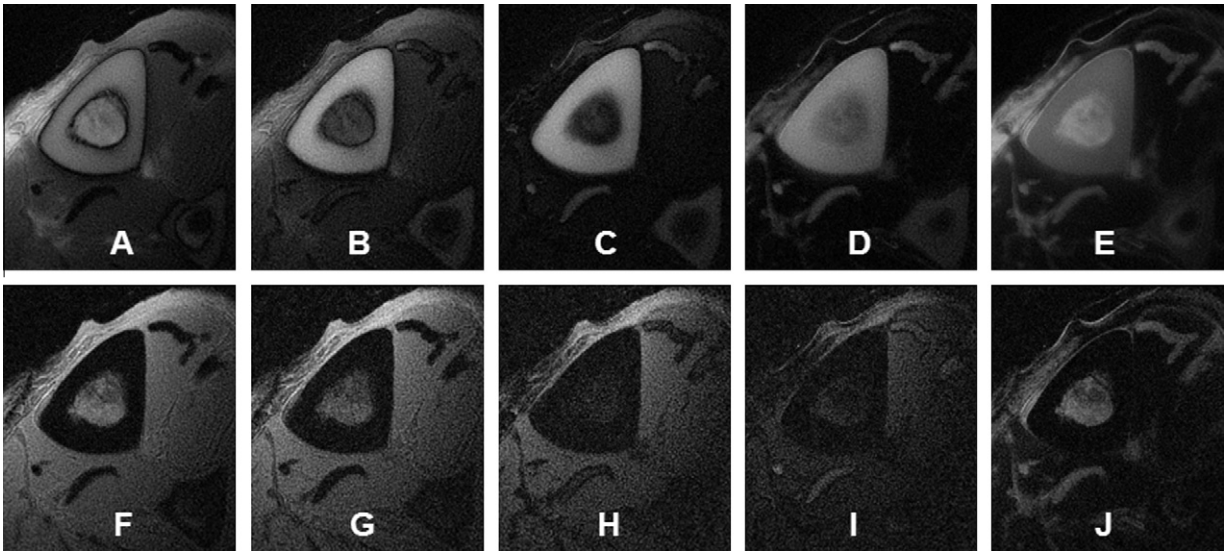

Fig. 3. Images of a mid-diaphyseal tibia specimen acquired with the IR-UTE sequence with a TR of 300 ms, TEs of 8 μs (1st row) and 4.4 ms (2nd row), and TI of 80 ms (A and F), 100 ms (B and G), 120 ms (C and H), 140 ms (D and I) and 160 ms (E and J). The second echo image selectively depicts the residual signals from long T_2 water and fat, reflecting long T_2 signal suppression effectiveness.

Table 2
Quantitative measurements of SNR for the mid-diaphyseal tibia in cadaveric specimens, CNR between bone and fat (CNR_{B_F}), and CNR between bone and muscle (CNR_{B_M}) for five different TR and TI combinations.

	TR = 300 ms, TI = 80 ms	TR = 300 ms, TI = 100 ms	TR = 300 ms, TI = 120 ms	TR = 300 ms, TI = 140 ms	TR = 300 ms, TI = 160 ms
SNR_B	24.21 ± 3.51	27.95 ± 3.68	29.52 ± 3.75	31.75 ± 3.64	34.90 ± 3.88
CNR_{B_F}	2.73 ± 034	18.46 ± 2.94	21.98 ± 3.15	11.92 ± 2.21	−10.68 ± 1.93
CNR_{b_m}	16.51 ± 2.18	22.37 ± 3.13	26.31 ± 3.46	29.41 ± 3.37	24.08 ± 3.59

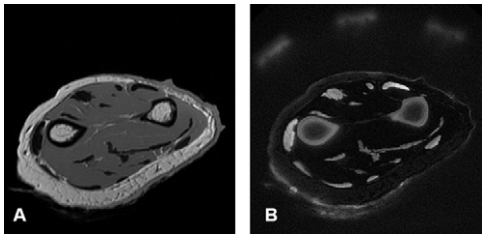

Fig. 4. A cadaveric forearm imaged with a clinical 2D FSE sequence (A) and an IR-UTE sequence (B). The 2D FSE sequence shows near zero signal for bone and tendon. These are depicted with high spatial resolution and contrast with the 2D IR-UTE sequence.

10-fold using the latter approach. These results suggest that fast and reliable estimations of T_1 and T_2^* of cortical bone can be achieved using protocol II.

4.3. In vivo volunteer study

Oblique axial images of the mid-diaphyseal tibia from four healthy volunteers are displayed in Fig. 6. For the first volunteer the IR-UTE image (Fig. 6C) was compared with 2D GE (Fig. 6A) and regular UTE images (Fig. 6B). The 2D GE sequence provides near zero signal for cortical bone. The 2D UTE sequence provides high signal for cortical bone with a SNR of 46 ± 5. However, there was little specific bone contrast due to the much higher signal from the surrounding muscle and marrow fat, resulting in a CNR_{B_M} of −65 ± 12 and CNR_{B_F} of −110 ± 11. The IR-UTE sequence provides a lower SNR of 30 ± 4, but much higher CNR_{B_M} (27 ± 3) and CNR_{B_F} (19 ± 3). The adiabatic IR pulse reduced bone signal by around 60%, roughly consistent with the Bloch equation simulation. However, it also reduced the background noise by around 40%, probably due to efficient suppression of signals from muscle and fat, therefore reducing pseudo-noise due to undersampling in the UTE data acquisition. As a result, the adiabatic IR pulse reduced bone SNR by 35% but increased CNR markedly.

Protocol II was used to measure T_2^* and T_1 for the mid-diaphyseal tibia of healthy volunteers. Fig. 7 shows typical IR-UTE images at different TEs. A short T_2^* of 408 ± 15 μs was found through a single exponential component curve fitting which accounted for 99.99% of the signal variance. The exponential T_2^* decay curve was barely affected by out-of-slice signal contamination, therefore increasing the accuracy and confidence in T_2^* quantification. Fig. 8 shows saturation recovery UTE imaging of the same volunteer. A short T_1 of 231 ± 17 ms was demonstrated by single exponential component curve fitting which accounted for 99.73% of the signal variance.

Fig. 9 shows results from bone water estimation using UTE and IR-UTE sequences. A water concentration of 22.2 ± 2.7% was found using regular 2D UTE imaging with bone appearing dark due to the high signal from the surrounding long T_2 muscle and fat. A slightly lower bone water concentration of 21.0 ± 2.3% was demonstrated using the 2D IR-UTE sequence with bone appearing bright after efficient reduction of long T_2 muscle and fat signals. The water concentration measured with the IR-UTE sequence was about 5.4% lower than that measured with the UTE sequence.

Table 3 lists the quantification of T_1, T_2^* and bone water concentration in the five healthy volunteers. The results show a mean T_1 of 223 ± 11 ms, a mean T_2^* of 390 ± 19 μs and a mean water concentration of 23.3 ± 1.6% assessed with UTE, and 21.7 ± 1.3% assessed with IR-UTE for the tibial cortex mid-shaft.

5. Discussion

It has been shown that the 2D UTE sequence combined with a long adiabatic IR preparation pulse can provide excellent qualitative depiction of cortical bone in vitro and in vivo using a clinical 3T scanner. The adiabatic IR pulse centered at −220 Hz has sufficient bandwidth to cover the water peak as well as the multiple

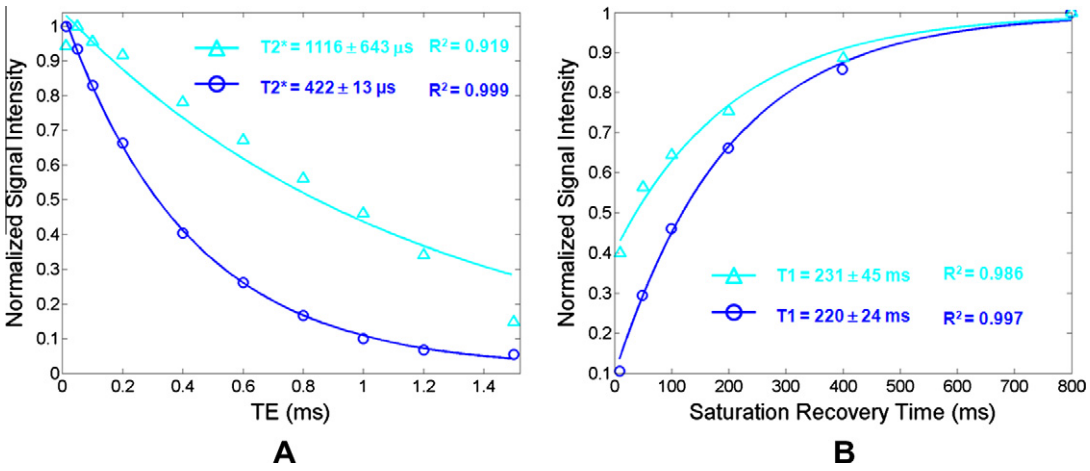

Fig. 5. Single component exponential decay curve fitting of T_2^* (A) and T_1 (B) for tibial cortical bone. This shows a short T_2^* of 1116 ± 643 μs (R^2 = 0.919) for tibia measured with UTE sequence and 422 ± 13 μs (R^2 = 0.999) measured with IR-UTE sequence, respectively (A). There is significant distortion and reduced confidence level in T_2^* fitting using the basic UTE sequence. Single component exponential recovery curve fitting shows a similar T_1 of 209 ± 52 ms and 200 ± 24 ms for the mid-diaphyseal tibia measured with saturation recovery UTE acquisitions with long and short TRs, respectively (B).

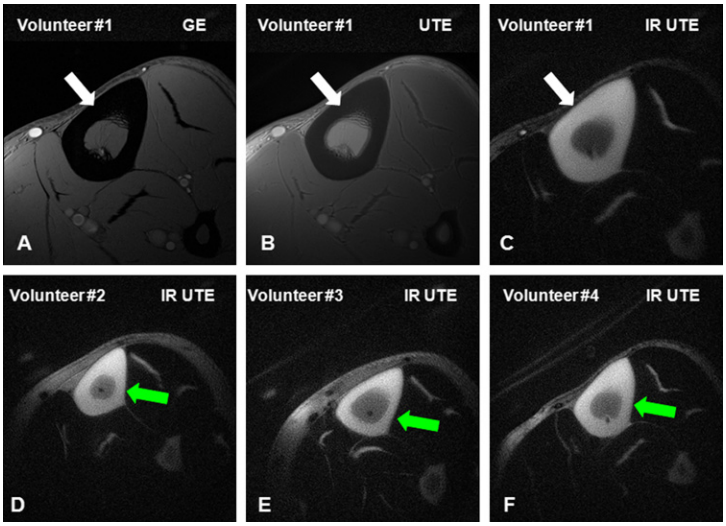

Fig. 6. The comparison of GE, UTE and IR-UTE sequences for imaging the tibia in human volunteers. Clinical GE sequence shows pure signal void for the mid-diaphyseal tibia (arrow) (A). This is also low signal with UTE due to the high signal from the surrounding long T_2 muscle and fat (arrow) (B). The IR-UTE sequence shows consistent high contrast images for cortical bone of four healthy volunteers (C–F). Long T_2 muscle and fat signals were efficiently suppressed through adiabatic inversion and approximate signal nulling.

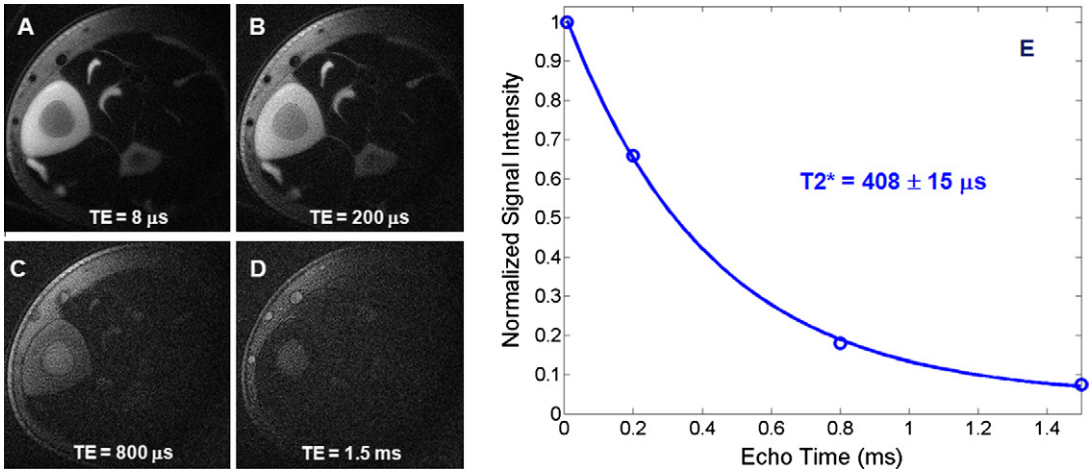

Fig. 7. IR-UTE imaging of the mid-diaphyseal tibia of a 31 year old healthy volunteer with a TE delays of 8 μs (A), 200 μs (B), 800 μs (C), and 1.5 ms (D). Mono-exponential fitting from a small ROI drawn in cortical bone demonstrates a short T_2^* of 408 ± 16 μs for this volunteer.

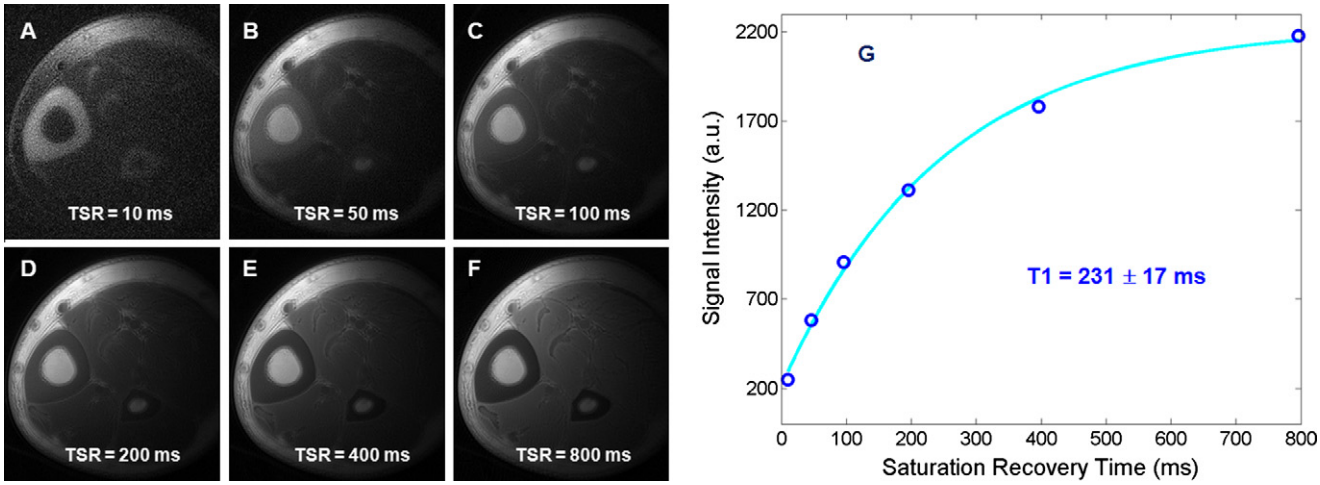

Fig. 8. Saturation recovery UTE imaging of the tibia of a 31 year old healthy volunteer with a TSRs of 10 ms (A), 50 ms (B), 100 ms (C), 200 ms (D), 400 ms (E) and 800 ms (F). Mono-exponential fitting from a small ROI drawn in cortical bone shows a short T_1 of 231 ± 17 ms (G).

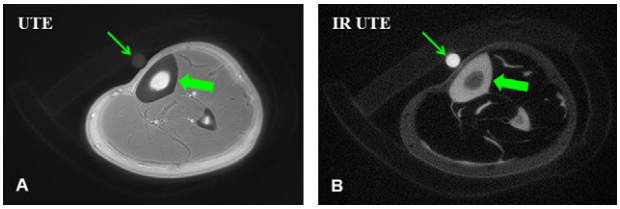

Fig. 9. Bone water concentration estimated by comparison of signal intensity of bone (thick arrows) to that of a water calibration phantom (thin arrows) using UTE (A) and IR-UTE (B) sequences. These gave water concentrations of 22.2 ± 2.7% and 21.0 ± 2.3%, respectively.

Table 3
Quantitative measurements of T_1, T_2^* and bone water content of mid-diaphyseal tibia in five healthy volunteers.

Subject	Age	T_1 (ms)	T_2^* (μs)	Bone water without IR (% volume)	Bone water with IR (% volume)
1	26	223 ± 22	376 ± 14	22.2 ± 2.7	21.0 ± 2 J
2	31	231 ± 17	408 ± 15	24.5 ± 2.9	22.6 ± 2.9
3	30	233 ± 18	412 ± 9	25.0 ± 33	23.3 ± 3.1
4	35	221 ± 21	387 ± 12	23.4 ± 2.8	21.7 ± 2.5
5	24	216 ± 20	369 ± 15	21.2 ± 2.4	20.1 ± 2.0

fat peaks in the spectral domain, and so provide uniform inversion of the long T_2 water and fat magnetization. Although only species with a specific T_1 can precisely reach the null point for each TR and TI combination, there are relatively broad ranges of TR and TI combinations which provide useful simultaneous signal reduction for both muscle and fat, as demonstrated in Figs. 2 and 3. The IR-UTE technique is robust, and provides high contrast bone images with little evidence of artifact from B1 and B0 inhomogeneities or susceptibility.

Fast and robust measurements of T_2^* and T_1 of cortical bone rely on the following factors. Firstly, an ultrashort nominal TE of 8 μs allows early points in the exponential curve to be sampled. This is especially important for cortical bone with its very short T_2^*. Secondly, the adiabatic IR pulse can robustly suppress long T_2 water and fat signals, and so minimize out-of-slice signal contamination as well as pseudo-noise associated with undersampled UTE acquisitions. This enhances the robustness of the T_2^* quantification technique (Figs. 5A and 7E). Thirdly, using a short TR as shown in protocol II, instead of the long TR shown in protocol I, the measurement time can be greatly reduced while maintaining reasonable agreement in T_1 quantification (Fig. 5B). Fourthly, undersampling can significantly reduce the total scan time with little effect on quantification, as demonstrated by the single component curve fitting shown in Figs. 5, 7 and 8.

Water occurs at various locations and in different states in cortical bone. It is associated with the mineral phase imbedded in the crystals of the apatite-like mineral [22] as well as the organic matrix, and is present in free form (bulk water) [16,22]. Measurement of bone water concentration may provide information on mineralization density and/or porosity. For example, Techawiboonwong et al. have compared the signal from bone and a water phantom to quantify bone water concentration as a new metric of bone quality in human cortical bone in vivo [6,12]. Cao et al. have also compared the signal from bone with a polymer calibration phantom, and found that the MR signal could be used to obtain true bone matrix mass density [23].

Our preliminary study shows a mean water concentration of 23.3 ± 1.6% assessed with the UTE sequence and 21.7 ± 1.3% assessed with the IR-UTE sequence for tibia of young volunteers. These values are broadly consistent with reported bulk water concentrations in cortical bone [6,12,24,25]. Precise agreement is unlikely due to the following factors: (i) out-of-slice long T_2 muscle and fat contamination may overestimate bone water concentration with UTE imaging. (ii) The T_1 and T_2^* relaxation times of bone water may have a broad spectrum of values [24,25]. Water in smaller pores and that closer to pore surfaces may have shorter T_1/T_2^* values due to surface relaxation mechanisms [26,27]. The single-component model used in T_1 and T_2^* fitting is only an approximation, and may result in errors in bone water estimation. Multi-component bone water quantification is much more complicated and is beyond the scope of this paper. (iii) The IR-UTE sequence may suppress the longer T_2 water components more than the shorter T_2 water components, resulting in an underestimation of T_2^* and increased errors in bone water quantification. However, the signal oscillation at early TEs in the T_2^* decay curve (Fig. 5A) without long T_2 signal suppression is probably due to out-of-slice long T_2 signal contamination. Lipids found in the cement line spaces may also contribute to this signal oscillation [30,31].

The effective TE in UTE imaging may be longer than the nominal TE due to radial ramp sampling, which is also likely to increase bone blurring [5]. Techniques such as sweep imaging with Fourier Transformation (SWIFT) and water- and fat-suppressed proton projection MRI (WASPI) may reduce bone blurring [9,28]. Another limitation of this study is that a single adiabatic IR pulse with relatively broad spectral bandwidth of 1.4 kHz was used. Adiabatic IR pulses with narrower spectral bandwidths are expected to reduce short T_2 signal attenuation [14], at the cost of increased sensitivity to field inhomogeneity and susceptibility effects. Another option is to use two adiabatic inversion pulses each with a much narrower spectral bandwidth to selectively invert and null long T_2 water and fat magnetization, respectively [29]. Furthermore, it is still not entirely clear whether bulk water, bound water, or both contribute to the signal detected by the UTE sequences. UTE imaging of bone samples after sequential dehydration, or sequential loss of bulk water and bound water [25], may provide such information and will be investigated in the future.

6. Conclusion

The 2D IR-UTE sequence is able to depict cortical bone with high spatial resolution, SNR and CNR on a clinical 3T scanner. Quantitative evaluation of T_2^*, T_1 and water concentration can be achieved in clinically acceptable scan times through appropriate combinations of UTE acquisition, long T_2 suppression, and projection undersampling strategies.

Acknowledgment

The authors thank grants support from GE Healthcare and RSNA Research Scholar.

Appendix A

With IR-UTE imaging, the short T_2 magnetization is partially inverted by the long adiabatic inversion pulse, and then partly excited by the half RF pulse [14,32]. The longitudinal magnetization $\mu_z(T_2)$ after the adiabatic IR pulse, neglecting T_1, will be approximately [14]:

$$\begin{aligned}\mu_z(T_2) &\approx \mu_0 \times (1 - T_2 \times \textstyle\int_{-\infty}^{\infty} \omega_1(t)^2 dt) \\ &\approx \mu_0 \times (1 - T_2 \times \textstyle\int_{-\infty}^{\infty} |\Omega_1(f)|^2 df) \\ &= \mu_0 \times (1 - P) = \mu_0 \times Q\end{aligned} \tag{A1}$$

Here P is the attenuation factor due to long adiabatic IR pulse.

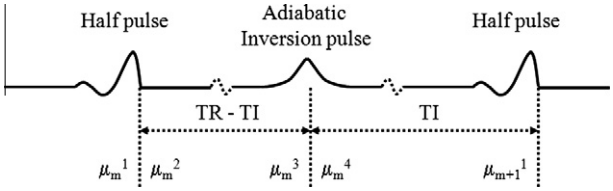

Fig. 10. Steady state magnetization of cortical bone with the IR-UTE sequence.

In order to obtain the steady state magnetization we introduced short T_2 magnetization at different stages of the IR-UTE pulse train (Fig. 10), namely before the half RF pulse (μ_m^1), after the half RF pulse (μ_m^2), before the adiabatic IR pulse (μ_m^3), after the adiabatic IR pulse (μ_m^4), and before the next half RF pulse (μ_{m+1}^1). Assuming a mapping matrix of f_z for the longitudinal magnetization and f_{xy} for the transverse magnetization, we obtain the following equations:

$$\mu_m^2 = \mu_m^1 \times f_z \tag{A2}$$

$$\mu_m^3 = \mu_0 + (\mu_m^2 - \mu_0) \times e^{-(\mathrm{TR}-\mathrm{TI})/T_1} \tag{A3}$$

$$\mu_m^4 = Q \times \mu_m^3 = Q \times [\mu_0 + (\mu_m^2 - \mu_0) \times e^{-(\mathrm{TR}-\mathrm{TI})/T_1}] \tag{A4}$$

$$\mu_{m+1}^1 = \mu_0 + [\mu_m^4 - \mu_0] \times e^{-\mathrm{TI}/T_1} = \mu_{ss} \tag{A5}$$

At steady state, $\mu_{m+1}^1 = \mu_{ss}$. Therefore we can obtain the following equation:

$$\begin{aligned}\mu_{ss} &= \mu_0 + \{Q \times [\mu_0 + (\mu_{ss} \times f_z - \mu_0) \times e^{-(\mathrm{TR}-\mathrm{TI})/T_1}] - \mu_0\} \times e^{-\mathrm{TI}/T_1} \\ &= \mu_0 + Q \times \mu_0 \times e^{-\mathrm{TI}/T_1} + Q \times \mu_{ss} \times f_z \times e^{-\mathrm{TR}/T_1} - Q \times \mu_0 \times e^{-\mathrm{TR}/T_1} - \mu_0 \times e^{-\mathrm{TI}/T_1}\end{aligned} \tag{A6}$$

As a result, μ_{ss} can be calculated as follows:

$$\mu_{ss} = \frac{\mu_0 \times [1 + (Q-1) \times e^{-\mathrm{TI}/T_1} - Q \times e^{-\mathrm{TR}/T_1}]}{1 - Q \times f_z \times e^{-\mathrm{TR}/T_1}} \tag{A7}$$

The mapping matrices f_z and f_{xy} are related to the half pulse profile and T_2^*. For slice selective half pulses, f_z and f_{xy} can be calculated by Bloch equation simulation. Since the reference water phantom and cortical bone have similar T_2^* values and T_1 effects can be ignored during half pulse excitation, it is reasonable to assume $f_{xy,bone} \approx f_{xy,ref}$, and $f_{z,bone} \approx f_{z,ref} = f_z$. The reference water phantom has a very short T_1. We can then calculate bone water concentration as follows:

$$\begin{aligned}\mathrm{BWC}_{\mathrm{IR-UTE}} &\approx \frac{\mu_{ss}^{bone} \times f_{xy}^{bone}}{\mu_{ss}^{ref} \times f_{xy}^{ref}} \times RWC \\ &\approx \frac{I_{bone}}{I_{ref}} \times \frac{1 + (Q_{ref} - 1) \times e^{-\mathrm{TI}/T_{1,ref}} - Q_{ref} \times e^{-\mathrm{TR}/T_{1,ref}}}{1 + (Q_{bone} - 1) \times e^{-\mathrm{TI}/T_{1,bone}} - Q_{bone} \times e^{-\mathrm{TR}/T_{1,bone}}} \\ &\quad \times \frac{1 - Q_{bone} \times f_z \times e^{-\mathrm{TR}/T_{1,bone}}}{1 - Q_{ref} \times f_z \times e^{-\mathrm{TR}/T_{1,ref}}} \times RWC \\ &\approx \frac{I_{bone}}{I_{ref}} \times \frac{1 - Q_{bone} \times f_z \times e^{-\mathrm{TR}/T_{1,bone}}}{1 + (Q_{bone} - 1) \times e^{-\mathrm{TI}/T_{1,bone}} - Q_{bone} \times e^{-\mathrm{TR}/T_{1,bone}}} \times RWC\end{aligned} \tag{A8}$$

References

[1] I.L.H. Reichert, M.D. Robson, P.D. Gatehouse, T. He, K.E. Chappell, J. Holmes, S. Girgis, G.M. Bydder, Magnetic resonance imaging of cortical bone with ultrashort TE (UTE) pulse sequences, Magn. Reson. Imaging 23 (2005) 611–618.

[2] A. Techawiboonwong, H.K. Song, F.W. Wehrli, In vivo MRI of submillisecond T2 species with two-dimensional and three-dimensional radial sequences and applications to the measurement of cortical bone water, NMR Biomed. 21 (2008) 59–70.

[3] C.J. Bergin, J.M. Pauly, A. Macovski, Lung parenchyma: projection reconstruction MR imaging, Radiology 179 (1991) 777–781.

[4] J.P. Wanspaura, B.L. Daniel, J.M. Pauly, K. Butts, Temperature mapping of frozen tissue using eddy current compensated half excitation RF pulses, Magn. Reson. Med. 46 (2001) 985–992.

[5] M.D. Robson, P.D. Gatehouse, M. Bydder, G.M. Bydder, Magnetic resonance. an introduction to ultrashort TE (UTE) imaging, J. Comput. Assist. Tomogr. 27 (2003) 825–846.

[6] J. Rahmer, P. Bornert, J. Groen, C. Bos, Three-dimensional radial ultrashort echo-time imaging with T2 adapted sampling, Magn. Reson. Med. 55 (2006) 1075–1082.

[7] J. Du, A. Takahashi, M. Bydder, C.B. Chung, Two dimensional ultrashort echo time imaging using a spiral trajectory, Magn. Reson. Imaging 26 (2008) 304–312.

[8] M.S. Sussman, J.M. Pauly, G.A. Wright, Design of practical T2-selective RF excitation (TELEX) pulses, Magn. Reson. Med. 40 (1998) 890–899.

[9] Y. Wu, J.L. Ackerman, D.A. Chesler, L. Graham, Y. Wang, M.J. Glimcher, Density of organic matrix of native mineralized bone measured by water- and fat-suppressed proton projection MRI, Magn. Reson. Med. 50 (2003) 59–68.

[10] P.E. Larson, P.T. Gurney, K. Nayak, G.E. Gold, J.M. Pauly, D.G. Nishimura, Designing long-T2 suppression pulses for ultrashort echo time imaging, Magn. Reson. Med. 56 (2006) 94–103.

[11] M.A. Fernandez-Seara, S.L. Wehrli, F.W. Wehrli, Multipoint mapping for semi-solid materials, J. Magn. Reson. 160 (2003) 144–150.

[12] A. Techawiboonwong, H.K. Song, M.B. Leonard, F.W. Wehrli, Cortical bone water: in vivo quantification with ultrashort echo-time MR imaging, Radiology 248 (2008) 824–833.

[13] M. Garwood, L. Delabarre, The return of the frequency sweep: designing adiabatic pulses for contemporary NMR, J. Magn. Reson. 153 (2001) 155–177.

[14] P.E. Larson, S.M. Conolly, J.M. Pauly, D.G. Nishimura, Using adiabatic inversion pulses for long-T2 suppression in ultrashort echo time (UTE) imaging, Magn. Reson. Med. 58 (2007) 952–961.

[15] A. Lu, B.L. Daniel, J.M. Pauly, K.B. Pauly, Improved slice selection for R2* mapping during cryoablation with eddy current compensation, J. Magn. Reson. Imaging 28 (2008) 190–198.

[16] F.W. Wehrli, H.K. Song, P.K. Saha, A.C. Wright, Quantitative MRI for the assessment of bone structure and function, NMR Biomed. 19 (2006) 731–764.

[17] S. Conolly, D. Nishimura, A. Macovski, G. Glover, Variable-rate selective excitation, J. Magn. Reson. 78 (1988) 440–458.

[18] J. Du, A.M. Takahashi, A. Shimakawa, M. Bydder, S. Sinha, G.M. Bydder. Ultrashort TE (UTE) imaging of the cortical bone at 3T, in: Proceedings of ISMRM 15th Annual Meeting, Berlin, Germany, May 2007, P381.

[19] J. Du, G. Hamilton, A. Takahashi, M. Bydder, C.B. Chung, Ultrashort TE spectroscopic imaging (UTESI) of cortical bone, Magn. Reson. Med. 58 (2007) 1001–1009.

[20] J. Du, A. Takahashi, M. Bydder, C.B. Chung, G.M. Bydder, Ultrashort TE imaging with off-resonance saturation contrast (UTE–OSC), Magn. Reson. Med. 62 (2009) 527–531.

[21] G.E. Gold, E. Han, J. Stainsby, G. Wright, J. Brittain, Beaulieu.C. Musculoskeletal, M. RI, At 3.0T: relaxation times and image contrast, AJR 183 (2004) 343–351.

[22] E.E. Wilson, A. Awonusi, M.D. Morris, D.H. Kohn, M. Tecklenburg, L.W. Beck, Highly ordered interstitial water observed in bone by nuclear magnetic resonance, J. Bone Miner. Res. 20 (2005) 625–634.

[23] H. Cao, J.L. Ackerman, M.I. Hrovat, L. Graham, M.J. Glimcher, Y. Wu, Quantitative bone matrix density measurement by water- and fat-suppressed proton projection MRI (WASPI) with polymer calibration phantoms, Magn. Reson. Med. 60 (2008) 1433–1443.

[24] Q. Ni, J.S. Nyman, X. Wang, A.D. Santos, D.P. Nicolella, Assessment of water distribution changes in human cortical bone by nuclear magnetic resonance, Meas. Sci. Technol. 18 (2007) 715–723.

[25] J.S. Nyman, A. Roy, X. Shen, R.L. Acuna, J.H. Tyler, X. Wang, The influence of water removal on the strength and toughness of cortical bone, J. Biomech. 39 (2006) 931–938.

[26] D.E. Woessner, An NMR investigation into the range of the surface effect on the rotation of water molecules, J. Magn. Reson. 39 (1980) 297–308.

[27] F. Hanus, P. Gillis, Relaxation of water absorbed on the surface of silica power, J. Magn. Reson. 59 (1984) 437–445.

[28] D. Idiyatullin, C. Corum, J.Y. Park, M. Garwood, Fast and quiet MRI using a swept radiofrequency, J. Magn. Reson. 181 (2006) 342–349.

[29] J. Du, A. Takahashi, W.C. Bae, C.B. Chung, G.M. Bydder, Dual inversion recovery, ultrashort echo time (DIR UTE) imaging: creating high contrast for short-T2 species, Magn. Reson. Med. 63 (2010) 447–455.

[30] S.C. Cowin, Bone poroelasticity, J. Biomech. 32 (1999) 217–238.

[31] R.A. Horch, J.S. Nyman, D.F. Gochberg, R.D. Dortch, M.D. Does, Characterization of 1H NMR signal in human cortical bone for magnetic resonance imaging, Magn. Reson. Med. (2010) (ahead of print).

[32] M. Carl, M. Bydder, J. Du, A. Takahashi, E. Han, Optimization of RF excitation to maximize signal and T2 contrast of tissues with rapid transverse relaxation, Magn. Reson. Med. 64 (2010) 481–490.